X-ray diffraction, extended x-ray absorption fine structure and Raman spectroscopy studies of WO_3 powders and $(1-x)WO_{3-y}\cdot xReO_2$ mixtures

A. Kuzmin[a] and J. Purans
Institute of Solid State Physics, 8 Kengaraga Street, LV-1063 Riga, Latvia

E. Cazzanelli
INFM and Dipartimento di Fisica, Università della Calabria, I-87036 Arcavacata di Rende (Cosenza), Italy

C. Vinegoni and G. Mariotto
INFM and Dipartimento di Fisica, Università di Trento, I-38050 Povo (Trento), Italy

(Received 11 May 1998; accepted for publication 24 August 1998)

Pure ground tungsten trioxide WO_3 and $(1-x)WO_{3-y}\cdot xReO_2$ mixtures were studied by x-ray absorption spectroscopy, x-ray powder diffraction and Raman spectroscopy in comparison with hydrogen bronzes H_xWO_3 and hydrogenated calcium tungstate $CaWO_4$:H. It was found that a grinding of pure WO_3 leads to a decrease of the crystallites size and a development of the bluish coloration. The color change was found to be reversible under moderate heat treatment or after storage in oxidizing atmosphere and is attributed to the reduced W^{5+} ions, located at the surface of freshly ground powder. The $(1-x)WO_{3-y}\cdot xReO_2$ mixtures were found to be composed of monoclinic/orthorhombic WO_3 and orthorhombic ReO_2 phases with a grain boundary containing reduced $W^{5.7+}$ ions which are mainly responsible for the compound color at low rhenium ion concentrations. In both cases, the $W^{(6-z)+}$ $(0<z\leqslant 1)$ color centers are responsible for strong optical absorption resulting in the dramatic decrease of the total Raman intensity. The structural models of free surface in pure ground WO_3 and bulk WO_3/ReO_2 intragrain boundary in $(1-x)WO_{3-y}\cdot xReO_2$ mixtures are proposed and discussed. © *1998 American Institute of Physics.* [S0021-8979(98)07322-8]

I. INTRODUCTION

Tungsten trioxide WO_3 is an important technological material widely known for its electrochromic[1] and catalytic[2] properties. These are determined by the ability of tungsten ions to change their valence state upon reduction/oxidation processes both in the bulk and at the surface of crystalline grains. In stoichiometric WO_3, the tungsten ions have the valence state $6+$ with the $5d$ shell being empty. The crystalline structure of tungsten trioxide is of distorted ReO_3 type and is composed of $[WO_6]$ octahedra joined by corners with tungsten ions being off-center due to the second-order Jahn-Teller effect.[3]

The defect-free WO_3 single crystals are transparent with a band gap about 2.9 eV at room temperature (RT), whereas commercial WO_3 powder has yellow or yellow-greenish color and appears to be *n*-type semiconductor due to the presence of bulk defects.[4] When the valence state of tungsten ions is reduced, the oxide turns to be blue colored.[1] The color centers are generally attributed to defects consisting of electron charge excess, localized at the octahedra basic units $[W^{5+}O_6]$.[5] The blue coloration can be induced by different methods such as electrochemical insertion of small cations,[6,7] UV irradiation,[8–10] annealing in vacuum[11] and ion beam bombardment.[12] Besides, we have found recently that freshly ground WO_3 powder also has bluish color whose intensity depends on the grinding time.[13] It is also possible to stabilize the tungsten in the valence state $5+$ by the presence of other oxides, as for example in the $(1-x)WO_{3-y}\cdot xReO_2$ system.[13]

Depending on the reduction method, the W^{5+} color centers can be found in the bulk or at the surface of crystalline grains. Moreover, depending on the concentration of such centers, the additional $5d$ electron can be localized (small polaron) or delocalized on few (large polaron) or infinite (conductive electron) number of tungsten ions.[3] Most works up to now were devoted to the study of bulk color centers with localized (as in amorphous thin films or glasses) or delocalized (as in bronzes) $5d$ electrons.[1,3,14] However, recent applications of the scanning tunneling microscopy (STM)[15,16] allowed to probe the free surfaces of $Na_{0.65}WO_3$ and WO_3 crystals and to study their reconstruction upon annealing in ultrahigh vacuum at the atomic scale. In both cases, one deals with a WO_2 surface layer with half a monolayer of oxygen ions, and electrical neutrality is maintained by the tungsten ions reduced from W^{6+} to W^{5+} with a localized $5d^1$ electron configuration.[15,16]

Thus, the presence of reduced tungsten ions in a compound is one of the main responsible for its physical properties such as optical absorption, catalytic activity and electron conductivity. Therefore the study of such centers is of great interest from both fundamental and applied points of view. In the past, the W^{5+} centers were mainly probed by electron spin resonance (ESR) technique, optical absorption and x-ray photoelectron spectroscopy (XPS).[1] All three methods provide mainly information on the electronic structure of the

[a]Electronic mail: xas@latnet.lv

W^{5+} centers, whereas their direct structural investigations[17] are usually difficult due to small concentration of the reduced sites compared to the total number of tungsten ions in a compound. Therefore, one can expect to elucidate more by using a combination of different direct and indirect structural techniques applied to the same samples.

In this work, we present a complex structural study by x-ray diffraction (XRD), extended x-ray absorption fine structure (EXAFS), and Raman spectroscopy of free surface in pure ground WO_3 and bulk intragrain boundaries in $(1-x)WO_{3-y}\cdot xReO_2$ mixtures in comparison with hydrogen bronzes H_xWO_3 and hydrogenated $CaWO_4$:H. We propose two structural models (free surface model and bulk intragrain boundary model) which take into account modifications of both atomic and electronic structures around tungsten ions.

The article is organized as follows: in Sec. II, the details of different samples preparation and experimental techniques as EXAFS, XRD and Raman spectroscopy are described; in Sec. III, main results and correlations between them found by different techniques are discussed, and two structural models, free surface model for ground WO_3 and bulk intragrain boundary model for $(1-x)WO_{3-y}\cdot xReO_2$ mixtures, are proposed; in Sec. IV, the summary of the work and main conclusions are presented.

II. EXPERIMENT

A. Sample preparation

The starting compounds used in the present work were commercial WO_3 (yellow), ReO_3 (dark-red) and $CaWO_4$ (white) powders with a nominal purity of 99 to 99.99%. From these powders different sets of samples have been obtained and studied separately. The ''as-purchased'' powders will be called in the following as ''virgin'' powders.

It was found by our XRD and Raman measurements[13] that commercial WO_3 powder, which underwent a mild milling procedure consisting of a manual compression in a mortar of agate for a few minutes, structurally differs from the virgin WO_3 powder. This kind of powder will be labeled as ''treated powder.''

A set of samples was produced from the virgin WO_3 powder by mechanical grinding using a Retschmuele ball milling machine. Three balls of agate having diameters between 0.5 and 1 cm and weight between 0.17 and 1.09 g were used. The working frequency was of the order of 1 Hz (50–70 cycles per minute), and the grinding time was in the range from a few minutes up to 21 h. The samples obtained by means of this treatment will be referred as ''ground powders.'' It is important to note that *freshly* ground powders were bluish colored with the color density being stronger for longer time of grinding.

Hydrogenated samples with a general composition H_xWO_3 were prepared by H^+ insertion to the virgin WO_3 powder placed in 1 N aqueous solution of sulfuric acid in the presence of indium as catalyst. The hydrogen content was estimated by comparison of x-ray powder diffraction patterns for our samples with that available in the literature. The as-prepared samples had deep-blue color and the composition $x=0.23$ corresponding to the tetragonal phase[14] (JCPDF-ICDD 20-483). Upon hydrogen loss, they transformed first into orthorhombic H_xWO_3 phase, with $x=0.1$ (JCPDF-ICDD 6-210), and later turned into monoclinic (I) WO_3.

A series of $(1-x)WO_{3-y}\cdot xReO_2$ mixtures was prepared from variable amounts of WO_3 and ReO_3 starting powders. In the chemical formula, the index x denotes the relative molar fraction of rhenium ions, and the index y reflects the nonstoichiometry of the final product. Note that the use of this notation does not imply the formation of a new phase of a mixed crystal or a solid solution, however, we cannot exclude from our data a possibility for partial (less than 1%) incorporation of Re or W ions into tungsten or rhenium rich phase, respectively. The starting oxide materials were finely ground in air by manual grinding for some minutes, and then sealed under vacuum in quartz ampoules, which underwent successive heating for 17 h at 450 °C and then for 73 h at 600 °C. After the thermal treatments, the powders were again reground manually in air. Following this procedure seven different samples were obtained with a composition in the range $0<x<1$. Their color was varied from grayish-blue to black. Since rhenium trioxide decomposes in vacuum into solid ReO_2 and gaseous Re_2O_7 at about 400 °C, the true molar composition (x) and the phase content of the $(1-x)WO_{3-y}\cdot xReO_2$ mixtures was different from the molar ratio of starting oxides. The x value was determined by x-ray absorption spectroscopy (XAS) from the ration of the W and Re L_3 edge jumps (see Sec. II C): it was equal to 0.05, 0.11, 0.17, 0.21, 0.24, 0.51 and 0.81. XRD was used to determine the phase composition (see Sec. II B): the presence of two phases (WO_3 and ReO_2) was found.

Finally, hydrogenated $CaWO_4$:H samples were prepared using the same procedure as for H_xWO_3 bronzes, i.e., the hydrogen insertion has been performed in the 1 N solution of sulfuric acid in the presence of metallic indium as catalyst. The fresh $CaWO_4$:H were deep-blue colored. No change in the phase of $CaWO_4$ upon hydrogen insertion was detected by our XRD measurements. The hydrogen doped $CaWO_4$:H samples were unstable and turned back to $CaWO_4$ after several hours of exposure to air.

B. XRD measurements

X-ray powder diffraction patterns of ground WO_3 powders [Fig. 1(a)] and $(1-x)WO_{3-y}\cdot xReO_2$ mixtures [Fig. 1(b)] were recorded using a Bragg-Brentano-type diffractometer (ItalStructures) with a graphite monochromator in the diffracted beam for elimination of sample fluorescence. Conventional tube with copper anode (Cu $K\alpha$ radiation) was used as x-ray source. The measurements ($\theta/2\theta$ scans) were performed at room temperature (RT) in the angle range $2\theta=20-65°$ and a step $\Delta(2\theta)=0.05°$. The samples for XRD were prepared (a) by mounting a powder in the standard sample holder made of copper or (b) by deposition of the powder on a Millipore filter from an aqueous suspension driven by a vacuum pump.

C. EXAFS measurements

X-ray absorption spectra (Fig. 2) of the W and Re L_3 edge in $(1-x)WO_{3-y}\cdot xReO_2$ mixtures and pure WO_3 were

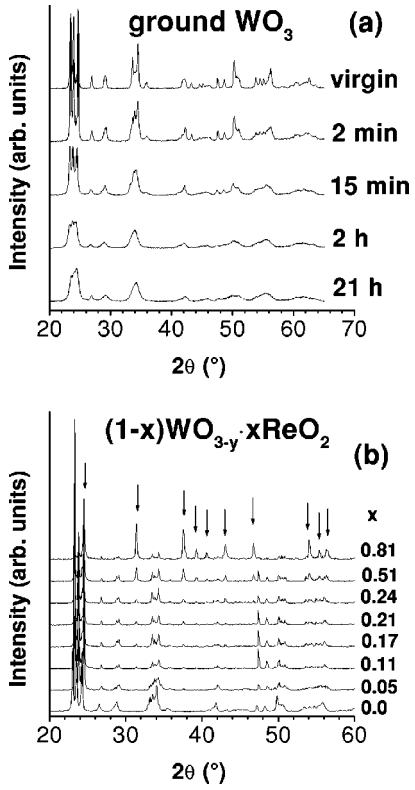

FIG. 1. (a) XRD patterns of ground WO_3 powder as a function of the milling time from 2 min to 21 h. Note that virgin WO_3 powder is in the monoclinic (I) phase whereas the one ground for 2 min is in the triclinic phase. A strong broadening of XRD patterns occurs at longer milling time due to a decrease of the grains size. (b) XRD spectra of $(1-x)WO_{3-y}\cdot xReO_2$ mixtures for various compositions. The XRD pattern for $x=0$ corresponds to triclinic WO_3 phase. For $x>0.05$, the peaks (marked by arrows) of the ReO_2 phase are visible, additionally to those of WO_3 which transforms to the orthorhombic-type phase.

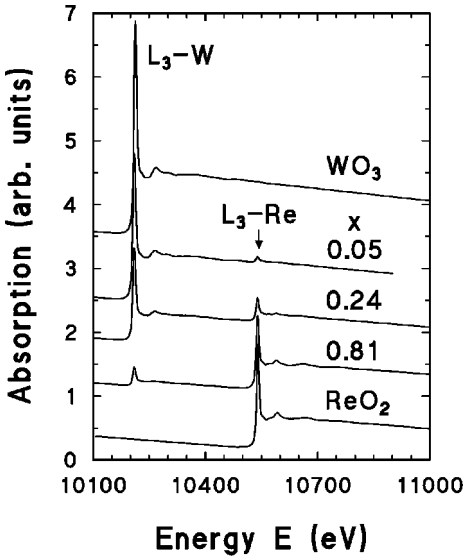

FIG. 2. Experimental x-ray absorption spectra of the W and Re L_3 edge in $(1-x)WO_{3-y}\cdot xReO_2$ mixtures. Only few signals are shown for clarity. The spectra of pure WO_3 and ReO_2 are shown for comparison.

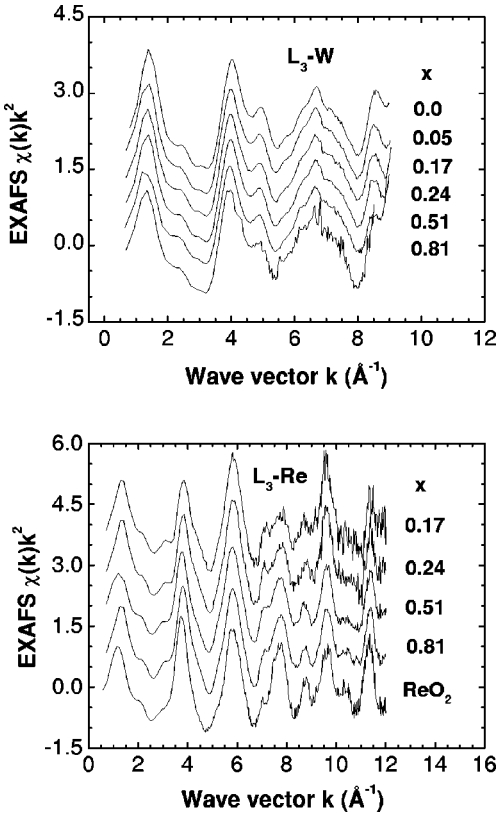

FIG. 3. Experimental EXAFS $\chi(k)k^2$ spectra of the W and Re L_3 edge in $(1-x)WO_{3-y}\cdot xReO_2$ mixtures. The data for pure WO_3 ($x=0$) and ReO_2 crystals are shown for comparison.

recorded at the LURE DCI storage ring on the EXAFS-3 beamline located at the bending magnet. The storage ring DCI operated at the energy 1.85 GeV, at a maximum stored current 316 mA. A standard transmission scheme with a Si(311) double-crystal monochromator and two ion chambers containing argon gas was used. The measurements were done at room temperature. The EXAFS (Fig. 3), located above the edge, was extracted using the EDA software package[18] following the standard procedure.[19] The ratio of the W to Re L_3 edge jumps $\Delta\mu(L_3-W)/\Delta\mu(L_3-Re)$ was used to determine the true content of the $(1-x)WO_{3-y}\cdot xReO_2$ compounds.

D. Raman measurements

The Raman measurements were performed in backscattering geometry using a microprobe setup, consisting of an Olympus microscope (model BHSM-L-2), mounting an objective 80× with a numerical aperture NA=0.75 and coupled to an 1 m focal length double monochromator Jobin-Yvon (Ramanor, model HG2-S) equipped with holographic gratings (2000 grooves/mm). The spectral resolution was of the order of 3 cm^{-1}. The scattered radiation was detected by a cooled (−35 °C) photomultiplier tube (RCA, model C31034A-02), operated in photon counting mode. The signal was stored into a multichannel analyzer and then sent to a microcomputer for the analysis. The spectra shown in Figs. 4, 5(a) and 9 were excited by the 530.9 nm (yellow-green) line of a Krypton laser. The spectra presented in Fig. 5(b)

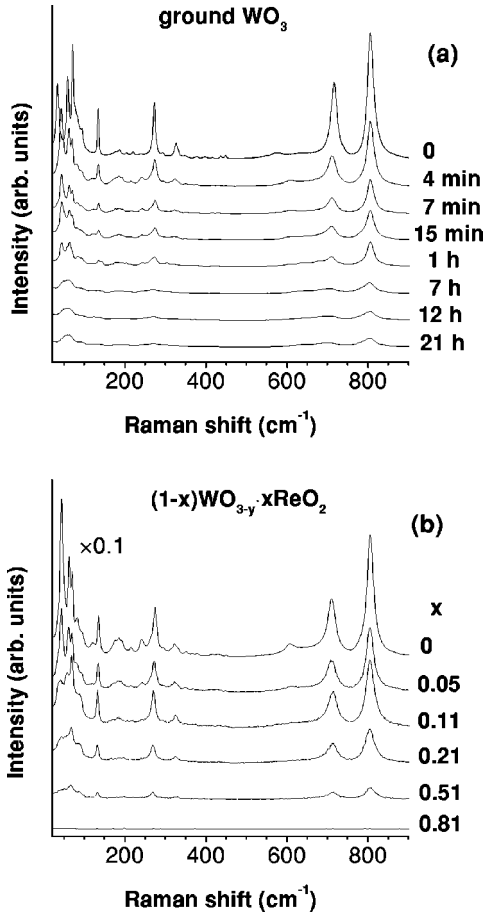

FIG. 4. (a) Raman spectra ($\lambda_{ex}=530.9$ nm) of ground WO_3 powder as a function of the milling time. A decrease of the Raman intensity and an increase of the Raman bands broadening occur with increasing time of the milling. (b) Raman spectra (exciting wavelength was 530.9 nm) of $(1-x)WO_{3-y}\cdot xReO_2$ mixtures for various compositions x. The intensity of the upper spectrum, corresponding to the treated WO_3 powder ($x=0$) was reduced ten times.

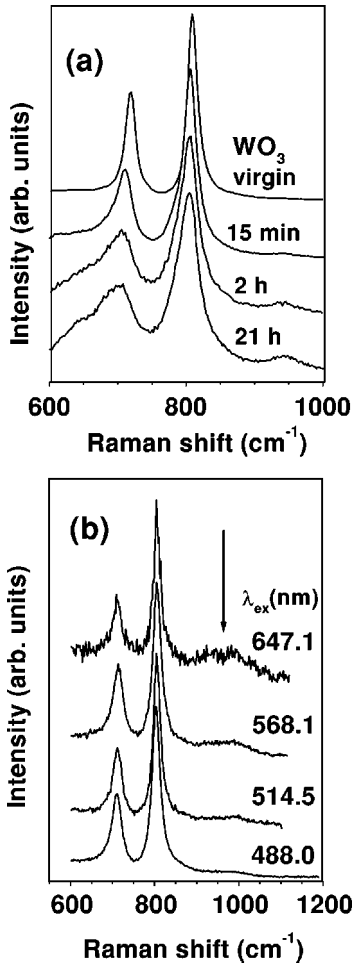

FIG. 5. (a) Variation of the Raman band at $\sim 950\ cm^{-1}$ in ground WO_3 powders relative to the stretching mode at $800\ cm^{-1}$ as a function of the milling time. While the total intensity of the Raman signal decreases with increasing time of the milling [see Fig. 4(a)], the relative intensity of the band at $\sim 950\ cm^{-1}$ increases. (b) Raman spectra of $0.95WO_{3-y}\cdot 0.05ReO_2$ mixture excited with different wavelength lasers. The Raman intensity was normalized to the band at $800\ cm^{-1}$. The resonance effect is visible for the band at $\sim 970\ cm^{-1}$: its intensity is higher for the excitation in the red spectral range ($\lambda_{ex}=647.1$ nm).

were excited by the 488.0 (blue) and 514.5 (green) lines of an Argon laser and 568.1 (yellow) and 647.1 nm (red) line of a Krypton laser. The spectra shown in Fig. 6 were excited by (a) the 530.9 nm and (b) 568.0 nm lines of a Krypton laser. The lasers were operated so that the power entering in the microscope was maintained below 10 mW for the 488.0 and 514.5 nm lines, 20 mW for the 530.9 nm line and 60 mW for 568.1 and 647.1 nm lines.

III. RESULTS AND DISCUSSION

A. Ground WO_3

X-ray powder diffraction patterns of ground WO_3 powders are shown in Fig. 1(a). Significant broadening of the Bragg peaks occurring upon increasing of the grinding time is observed and is attributed to a decrease of the crystalline grain size. Our estimate, using the conventional Scherrer method,[20] suggests that the relative size was reduced about five times during the first two hours and no further reduction of crystallites dimensions has occurred in our experimental conditions for longer times of grinding [Fig. 7(a)]. This result is consistent with the fact that no amorphization can be achieved in tungsten trioxide using mechanical grinding as was observed in Ref. 21

One can also note that at initial stages of grinding [see patterns of virgin and 2 min ground WO_3 in Fig. 1(a)], the phase transformation from monoclinic to triclinic phase rapidly occurs at ambient temperature.[22] This transition can be easily followed by looking the evolution of low frequency bands (up to $100\ cm^{-1}$) in the Raman spectra [Fig. 4(a)]. The low frequency bands are attributed to the external modes. They are noticeably affected by the transitions between the low symmetry phases of WO_3, which involve mainly collective rotations of the basic [WO_6] octahedral units.[22,23] The larger sensitivity of the Raman spectra for the monoclinic-to-triclinic transition compared to XRD is related to the fact that the XRD patterns are mainly sensitive to the tungsten atoms positions, which negligibly change during the transition. The Raman spectra show different features in the monoclinic and triclinic phases:[23] in particular, the relative

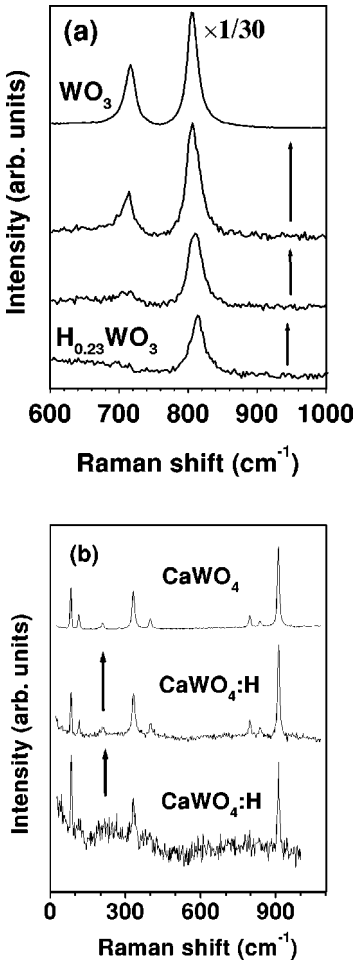

FIG. 6. Raman spectra of hydrogenated (a) H_xWO_3 and (b) $CaWO_4$:H compounds. Note that upon hydrogen loss, the total intensity of the Raman signals increases in both cases. Besides, H_xWO_3 powder transforms from tetragonal $H_{0.23}WO_3$ to orthorhombic $H_{0.1}WO_3$ and, finally, to monoclinic (I) WO_3 phase whereas the phase of tungstate does not change, being always tetragonal as of pure $CaWO_4$ (see Ref. 26).

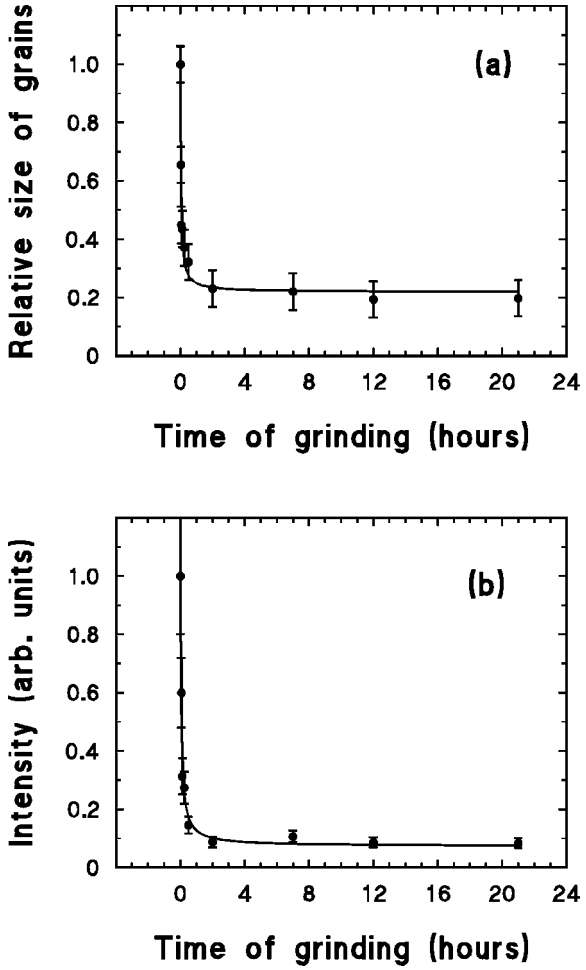

FIG. 7. Variation of (a) the relative grain size and (b) Raman intensity in pure ground WO_3 as a function of the grinding time. The solid lines are guides for the eye. Note that Raman spectra were taken from freshly ground powders. The correlation between two phenomena shown in (a) and (b) is explained by the damping of the Raman intensity at the color centers W^{5+} created by the grinding process and located at the fresh surfaces of grains.

intensity of the 34 cm^{-1} peak (typical of monoclinic phase) decreases and that of the 41 cm^{-1} peak (typical of triclinic phase) increases [Fig. 4(a)].

Upon the increase of the grinding time to many hours, a further variation of the Raman spectra occurs and is mainly related to a broadening of the bands and a decrease of the total Raman intensity. Both effects are well visible in Fig. 4(a). We should point out that all spectra were recorded on freshly ground powders having bluish color of different intensity. As has been mentioned in Sec. II A, the powders experiencing longer grinding time were deeper colored.

The variation of the Raman intensity for freshly ground powders as a function of the grinding time is shown in Fig. 7(b). It can be observed that Raman intensity decreases rapidly during first two hours of the treatment and remains unchanged for longer times. By comparing Figs. 7(a) and 7(b), one might expect that the two phenomena, i.e., decrease of the grain size and Raman intensity, are strongly correlated. However, this conclusion is misleading and can be ruled out by the following experiment.

In Fig. 8, we show the XRD patterns for two arbitrary samples which were measured on freshly ground powders and after their treatment in air at moderate temperature $T = 90\ °C$ for 8 h. One can see that no difference is observed in the XRD patterns for fresh and thermally treated grounded powders. This means that the average grain size remains unchanged. However, the color of both samples was different, i.e., bluish before and yellow after heat treatment. Such change of color was observed for all powders being ground for different time and heat treated after that, as well as for ground powders stored at RT in air for a long time. In contrast to the XRD results, the Raman spectra of fresh and thermally treated ground powders were found to be different (dashed and dotted curves in Fig. 9, respectively). Moreover, it was observed that upon heat treatment the intensity of the Raman signal increases and the spectrum becomes close to that of starting treated WO_3 powder (solid curve in Fig. 9). Finally, we conclude that the changes in the XRD patterns are mainly due to a decrease of grains size that is not reversible at moderate temperature treatments. On the contrary, the changes in the Raman spectra intensity are determined

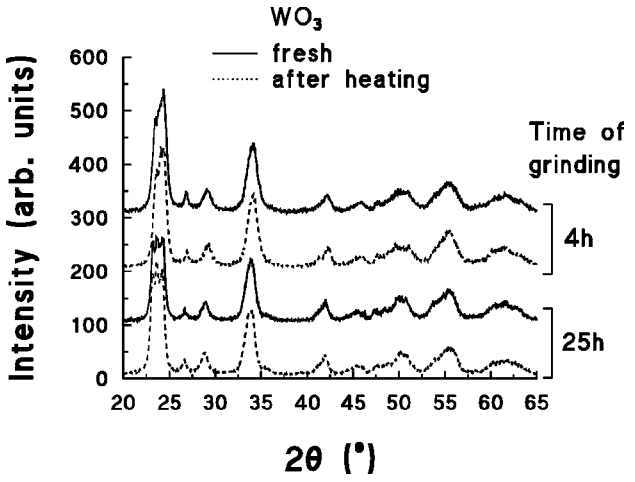

FIG. 8. XRD patterns of ground WO_3 powders: solid lines—freshly ground (bluish color), dashed line—after heating in air for 8 h at 90 °C (yellow color). Note that no change in the grain size occurs after moderate heat treatment, while the color of the powder changes from bluish to yellow.

mainly by the bluish coloration of the powder, which is reversible against heat treatment in oxidizing atmosphere. The effect of the grains size on the total Raman intensity appears as a small decrease due to bands broadening and is weaker compared to the effect of coloration.

It is interesting to note that upon extensive grinding a new Raman band is growing at about 940 cm^{-1} [Fig. 5(a)]: it can be observed already after 15 min of grinding. The band increases its relative intensity with increasing time of grinding in spite of the total Raman intensity decreases and becomes very well visible in the Raman spectrum of the sample ground for 21 h. This band remains nearly unchanged upon moderate heat treatments, which result in the reconstruction of the total Raman intensity. Therefore we attribute the presence of the 940 cm^{-1} band to surface tungsten–oxygen bonds whose relative number increases with a decrease of grains size.

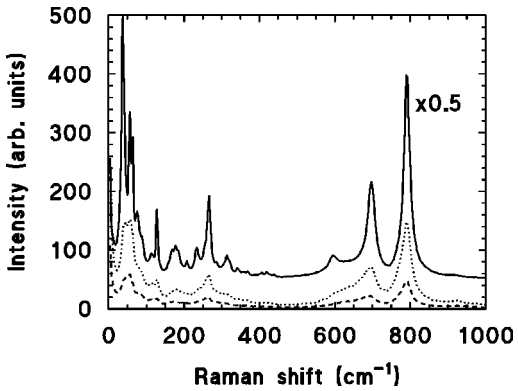

FIG. 9. Raman spectra of the same sample of WO_3: solid line (intensity was decreased two times)—starting treated powder (yellow color), dashed line—after 1 h of milling (bluish color), dotted line—after storing for 8 h in air at 90 °C (yellow color). Note that the color of the ground powder returns upon oxidation to those of starting treated powder. Also the Raman intensity of the ground powder increases upon oxidation but remains weaker than that of starting treated powder due to the difference in the grain size.

B. Hydrogenated H_xWO_3

The tungsten trioxide powder transforms upon hydrogen insertion into deep-blue colored hydrogen bronze H_xWO_3 which has the tetragonal phase for the hydrogen content $0.15<x<0.50$.[24] However, this tungsten bronze is unstable against oxidizing atmosphere so that the powder returns back to yellow monoclinic (I) WO_3 phase, passing through the orthorhombic H_xWO_3 $(0.1<x<0.15)$, during exposition in air for a long enough time.[24] In our case, the initial hydrogen content was estimated from XRD data to be about 0.23 and the evolution of the Raman spectra in the high-frequency region upon hydrogen loss is shown in Fig. 6(a).

Because of the fast de-hydrogenation process occurring during the Raman measurements, no quantitative estimation of the hydrogen content was possible for intermediate compositions. However, the time sequence of the spectra in Fig. 6(a) corresponds to a decrease of x from 0.23 to 0. To minimize systematic errors, the spectra were collected very rapidly, losing somewhat in the signal-to-noise ratio. Besides, the data acquisition for all spectra was started from the higher frequency side to avoid a bias in the intensity ratio of 710–816 cm^{-1} bands which depresses the lower frequency mode upon de-hydrogenation process. In fact, the 710 cm^{-1} mode decreases strongly with respect to the 816 cm^{-1} mode upon hydrogen insertion, and disappears [Fig. 6(a)] for proton concentrations lower than the maximum attainable ($x \simeq 0.23$). The above mentioned experimental procedure insures that the effect is true.

The observed variation in the number of Raman bands upon hydrogen loss is consistent with the structural transformation from tetragonal to orthorhombic and finally monoclinic phase.[24] Note that the 816 cm^{-1} stretching mode remains observable even for the highest proton content, corresponding to the tetragonal $H_{0.23}WO_3$ phase.

Besides the modifications of the Raman spectra related to the phase transition, strong changes were observed in the total intensity of the Raman signal for hydrogenated samples. This effect is attributed to the optical absorption effect caused by the blue color centers, appearing with the proton insertion and associated with reduced tungsten ions in the $(6-x)+$ valence state. The injected electrons occupy the $5d$ states of tungsten ions and have delocalized character being responsible for metallic conductivity of tungsten bronzes.[3]

An interesting aspect of the Raman spectra evolution in H_xWO_3 is a dependence of the highest stretching mode frequency on hydrogen content [Fig. 6(a)]: upon dehydrogenation, its frequency decreases from 814 cm^{-1} in $H_{0.23}WO_3$ to 806 cm^{-1} in monoclinic (I) WO_3. Such a behavior is not expected from the variation of the W–O bond length, since the latter becomes longer in bronze with higher proton content and, therefore, one would think about a decrease of the W–O stretching frequency. However, this picture does not take into account the change in the valence state of tungsten ions, which works in the opposite direction, so that for more reduced state one expects stronger bonding between tungsten and oxygen ligands. The interplay of these two effects results in the behavior observed experimentally.

C. $(1-x)WO_{3-y}\cdot xReO_2$ mixtures

X-ray diffraction was used to study the long range order in the mixture of compounds with the aim to check for the formation of either solid solution or multiphase system [Fig. 1(b)]. The powder diffraction patterns of $(1-x)WO_{3-y}\cdot xReO_2$ can be interpreted by assuming the presence of two phases: (1) tungsten trioxide WO_3 with monoclinic symmetry at $x=0.05$ and monoclinic/orthorhombic symmetry at $x>0.05$ and (2) rhenium dioxide ReO_2 with orthorhombic symmetry which corresponds to the high-temperature rutile-type structure (JCPDF-ICDD 9-274). The evidence for the orthorhombic-type phase of WO_3, which exists at about 330 °C in pure oxide,[25] is strongly supported by the doubling of the relative intensity of the first diffraction peak at $2\theta=23°$. Thus, the mixture of two oxides stabilizes them into the phases occurring in pure state at high temperatures. Note also that diffraction peaks from the mixture are very narrow with widths being comparable to the pure tungsten trioxide [Fig. 1(b)]: this suggests the large grain size for each of phase and, thus, the large value of the ratio of the volume-to-surface atoms number.

However, since the sizes and electron structures of tungsten and rhenium ions are close, it remains unclear from XRD data if some substitution of tungsten by rhenium or vice versa is present within each of phase. To answer this question, the x-ray absorption spectroscopy was used.

The experimental x-ray absorption spectra of the W and Re L_3 edges are shown in Fig. 2. The variation of the ratio of the absorption jumps at two edges is well visible as a function of the composition. The small separation (about 320 eV) between two edges and the partial overlap between the EXAFS located above the tungsten edge with that above the rhenium edge do not allow to perform accurate analysis, however qualitative conclusions can be drawn from comparison with reference materials (WO_3 and ReO_2).

The extracted EXAFS signals are shown in Fig. 3. One can see that the noise in experimental data increases with a decrease of the ion (W or Re) content. A comparison of the EXAFS signals for the same edge shows their great similarity and allows to conclude that the average local structure around both tungsten and rhenium ions remains unchanged for different compositions. Further, it should be pointed out that the EXAFS signals of the mixtures at the W and Re edges are very similar to whose of pure WO_3 and ReO_2, respectively, suggesting closeness of their local structures.

Finally, the results obtained by the direct structural techniques as XRD and EXAFS suggest that $(1-x)WO_{3-y}\cdot xReO_2$ mixtures consist of two separate phases WO_3 and ReO_2. The interaction between the phases at grain boundaries stabilizes each other in orthorhombic symmetry existing in pure oxides at high temperature (>330 °C for WO_3 and >300 °C for ReO_2). As we will show below, this conclusion is also supported by the Raman spectroscopy.

The Raman spectra of the $(1-x)WO_{3-y}\cdot xReO_2$ series are shown in Fig. 4(b). All the observed vibrational modes in the frequency region from 20 to 900 cm^{-1}, for all mixtures, can be assigned to tungsten oxide dynamics. The Raman spectra in the mixtures with higher x seem rather similar to the spectra of pure WO_3 measured at temperatures well above the ambient one. The addition of rhenium oxide does not induce any remarkable change in the spectral shape, like the appearance of new bands, except a weak band at $\sim 970\ cm^{-1}$ discussed later. This fact suggests that no chemical reaction or formation of solid solution occur in the bulk of the crystal grains, and the rhenium-rich ReO_2 phase is not Raman active. This is not surprising since rhenium ions in ReO_2 are located in highly symmetrical environments and the oxide has metallic conductivity: both facts reduce strongly the Raman activity.

The most stricking effect observed in Raman spectra of $(1-x)WO_{3-y}\cdot xReO_2$ is related to the strong quenching of the Raman intensity upon increasing of the ReO_2 content [see the difference in the intensity of spectra for $x=0$ and $x\geqslant 0.05$ in Fig. 4(b)]. The presence of only 5% of ReO_2 decreases drastically the total Raman intensity by a factor of 20. Further increase of the ReO_2 content in the range from $x=0.05$ to $x=0.21$ additionally lowers the intensity by a factor of 2, and, finally, in the sample with $x=0.81$ no appreciable Raman signal is observed. Note that the dramatic intensity decrease versus x cannot be justified by the decrease of the tungsten oxide content.

Since all mixtures are colored from grayish-blue for low x values to black for high x values, and the color was found to be stable against oxidizing atmosphere, we suggest that the decrease of the Raman intensity is related to the formation of associated color centers, similar to the case of ground WO_3 powders (see before), with the reduced tungsten ions located at the tungsten oxide grain surfaces between WO_3 and ReO_2 phases. These color centers are supposed to be responsible for a quenching of the Raman intensity and their model will be discussed in Sec. III E.

Additional proof for the existence of such color centers in $(1-x)WO_{3-y}\cdot xReO_2$ is provided by the appearance in the Raman spectra of a new band at $\sim 970\ cm^{-1}$ [indicated by arrow in Fig. 5(b)]. The relative intensity of the band shows dependence on the wavelength λ_{ex} of the exciting light and increases with increasing λ_{ex} being the largest for the excitation with the red light ($\lambda_{ex}=647.1$ nm). It is well known[1] that reduced tungsten centers give an origin for the optical absorption band in the range from 0.5 to 3.0 eV with the maximum at $\sim 1.2-1.4$ eV. Therefore, the increase of the band intensity at $\sim 970\ cm^{-1}$ can be directly related to the resonance Raman effect, and, thus, its origin can be attributed to the W–O stretching modes at the reduced tungsten sites.

D. Hydrogenated $CaWO_4$:H

The Raman spectra for $CaWO_4$:H powder as a function of de-hydrogenation process are shown in Fig. 6(b). They were normalized to the intensity of the high-frequency band at 911 cm^{-1} corresponding to the W–O stretching mode.[26]

The total Raman intensity for the deep-blue colored powder [lower curve in Fig. 6(b)] was very low, that is well visible from the small signal-to-noise ratio in the experimental spectrum. During de-hydrogenation process, the color of the powder becomes lighter and the intensity of the Raman

signal increased [middle curve in Fig. 6(b)]. Finally, the powder took white color as those of pure $CaWO_4$, and the Raman spectrum turned to be very intense [upper curve in Fig. 6(b)].

It is important to note that all Raman bands at any stage of the de-hydrogenation process agree well with whose of pure $CaWO_4$,[26] and no additional bands were observed. Together with our XRD findings, this confirms that no change of phase occurs in $CaWO_4$ upon hydrogenation. However, the presence of hydrogen modifies the color of the powder from white to deep-blue and decreases strongly the total intensity of the Raman signal. It is known that the blue coloration of $CaWO_4$ is related to the presence of $[W^{5+}O_4]^-$ anions with reduced tungsten ions having localized $5d^1$ electron configuration.[27]

E. Structural models

The results obtained for ground WO_3, $(1-x)WO_{3-y}\cdot xReO_2$ mixtures, hydrogen bronzes H_xWO_3 and hydrogenated $CaWO_4$ can be summarized as follows: In all compounds, the appearance of bluish coloration leads to the strong decrease of the Raman intensity and is attributed to reduced tungsten ions. However, only in tungsten bronzes the presence of reduced tungsten ions results in the change of the crystalline phase well visible in XRD and Raman signals. In other cases, the additional electrons have localized nature and do not influence the crystal structure of the host. This is well supported by unchanged shapes of XRD, EXAFS and Raman data. It should be noted that the change of XRD patterns and broadening of Raman bands in ground WO_3 is attributed to the decrease of its grain size.

The interesting result observed in Raman spectra of ground WO_3 and $(1-x)WO_{3-y}\cdot xReO_2$ mixtures is related to the appearance of the new band at 950 and 970 cm^{-1}, respectively [Figs. 5(a) and 5(b)]. The frequency of the band corresponds well to that observed in crystalline tungsten hydrates and attributed to the short double terminal W═O bonds.[28] However, opposite to the case of hydrates, the present band is broad and has low intensity.

In ground WO_3, the intensity of the band at ~ 950 cm^{-1} increases with time of grinding and is nearly unchanged with respect to the moderate heat treatments. This fact together with the nearly unchanged shape of other Raman bands (excluding the effect of their broadening due to the decrease of the grain size) allows to attribute the high-frequency band to a vibration of the W–O bonds at the free surface of cracked grains. By taking into account, the bluish coloration of the freshly ground WO_3 powder, one can propose the following model of the free surface (Fig. 10).

We will consider a crack along the (100) crystallographic plane as an example. Due to the electrical neutrality condition, two situations can be present at the surface. In the first, half of tungsten atoms remain in the valence state $6+$ and are connected to the terminal oxygen ions giving one of their electron to the nearest tungsten ion which transforms into the W^{5+} state. This situation occurs at the free surfaces of $Na_{0.65}WO_3$ and WO_3 single crystals and was directly observed by an STM technique.[15,16] Moreover, the STM observations suggest the shortening of the terminal W^{6+}–O^- bond to the value about 1.6 Å that is close to the value of the W═O bonds in tungsten hydrates: this confirms the origin and the position of the band at ~ 950 cm^{-1} in ground WO_3 as suggested above. In the second situation, all tungsten atoms at the surface change their valence state to $5+$, and the surface is represented by a $W^{5+}O_2$ terminal layer. In both cases, the surface W^{5+} sites play the role of color centers and, being active, react with the oxidizing atmosphere (of air) leading presumably to a formation of the W^{6+}–OH bonds. The latter are responsible for the band at ~ 950 cm^{-1} in ground uncolored powders.

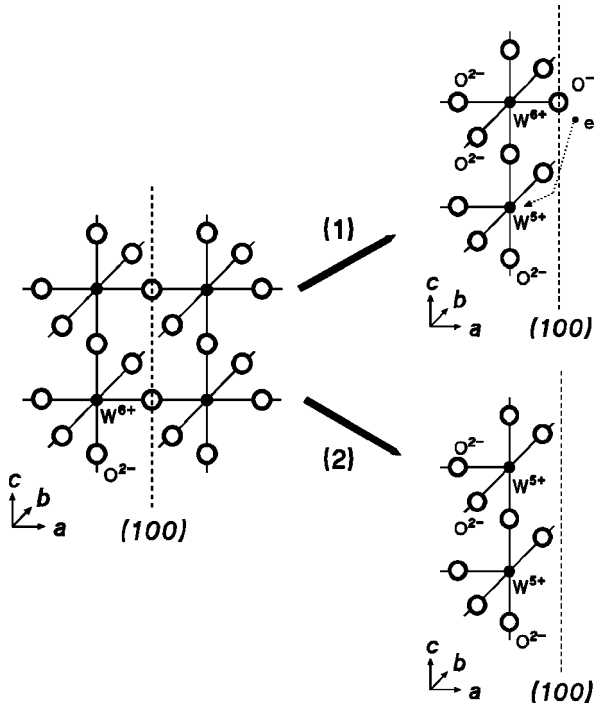

FIG. 10. Structural model of the color centers creation at the free grains surface in pure WO_3 upon milling. Left panel—idealized WO_3 structure with the (100) fracture plane shown. Right panel—two possible states of the fresh grains surface, formed upon milling: in both cases the formation of the reduced tungsten ions W^{5+} is required by the neutrality condition. The surface W^{6+}–O^- bonds with an expected length[15] of about 1.6 Å are supposed to give an origin of the Raman band at 950 cm^{-1} [Fig. 5(a)] in ground WO_3.

In the case of $(1-x)WO_{3-y}\cdot xReO_2$ mixtures, the color centers are stable against the oxidizing atmosphere. That allows to assume their location in the bulk; since the crystal structure of the WO_3 and ReO_2 regions remains the same at any rhenium content, one can think about the presence of the color centers at the bulk intragrain boundaries. Such model is presented in Fig. 11. Note that the crystal structure of the WO_3 phase is a distorted ReO_3 type and that of the ReO_2 phase is a rutile type. According to the electrical neutrality condition, the charge of the tungsten ions located at the boundaries between two phases should be lowered to $5.7+$, which transforms such sites into color centers. Moreover, the oxygen ion connecting two phases is bound to three ions—one tungsten ion $W^{5.7+}$ and two rhenium ions Re^{4+}. It is known[3] that in the rutile-type ReO_2 structure, the two rhenium ions are directly bound via $d(t_{2g})$ orbitals allowing for metallic conductivity along the chain made of $[ReO_6]$ octa-

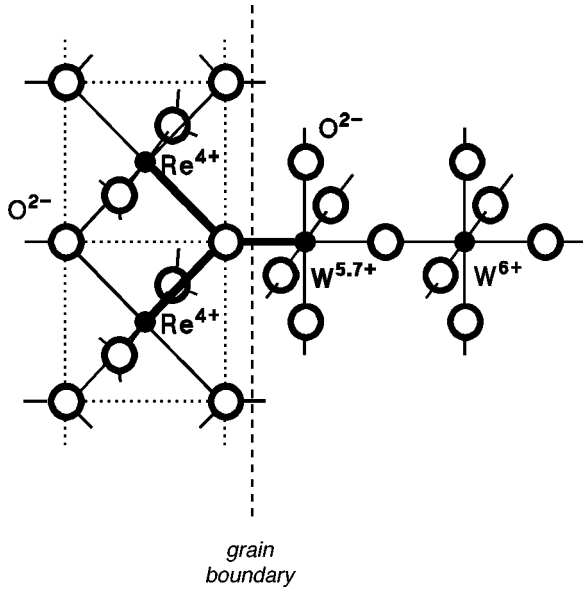

FIG. 11. Structural model of the color centers creation in $(1-x)WO_{3-y}\cdot xReO_2$ mixtures at the grains boundary between ReO_2 and WO_3 phases. The neutrality condition requires that the tungsten ions located close to the boundary becomes reduced to $W^{5.7+}$.

hedra joined by the edges. Therefore, one can expect that the oxygen ion is bound more strongly to $W^{5.7+}$ than to Re^{4+}. Also the intense color of the mixtures suggests that electrons located at $W^{5.7+}$ ions are highly localized, which also supports the strong bonding between oxygen and $W^{5.7+}$ ions. Thus, these $W^{5.7+}$–O bonds are expected to produce the 970 cm^{-1} band. Such interpretation is also supported by the resonance Raman effect observed for the 970 cm^{-1} band as shown in Fig. 5(b).

IV. SUMMARY AND CONCLUSIONS

In this work, we applied a combination of direct (x-ray absorption spectroscopy and XRD) and indirect (Raman spectroscopy) structural techniques to the study of pure ground WO_3 and $(1-x)WO_{3-y}\cdot xReO_2$ mixtures in comparison with hydrogen bronzes H_xWO_3 and hydrogenated $CaWO_4$.

The bulk structure of ground WO_3 resembles that of tungsten trioxide with grain size reduced up to five times depending on the grinding time. The bluish coloration of the freshly ground powders was observed and its intensity was deeper for longer time of grinding. It was also found that the color is not stable against moderate heat treatments or long time storage in an oxidizing atmosphere. The development of coloration upon grinding was related to the appearance of reduced tungsten ions at fresh surfaces of cracked crystal grains, and the model of such process was proposed (Fig. 10).

The $(1-x)WO_{3-y}\cdot xReO_2$ mixtures were found to be composed of monoclinic/orthorhombic WO_3 and orthorhombic ReO_2 phases. The size of crystal grains for both phases is comparable to that of pure oxides. However, the phases are interconnected forming bulk intragrain boundaries whose model is proposed (Fig. 11). The boundary region is composed of reduced tungsten ions which are mainly responsible for the coloration of the mixture at low rhenium concentrations. It should also be noted that contrary to the ground WO_3, the color of the mixture is stable against oxidizing atmosphere at temperatures well above the ambient one.

It was observed that in both cases the presence of reduced tungsten ions influences strongly the optical properties of the material and decreases the total intensity of the Raman signal. A similar effect was found in hydrogen bronzes H_xWO_3 and hydrogenated $CaWO_4$. Besides the intensity variation, it is concluded that in the case of small numbers of reduced tungsten sites with localized $5d^1$ electron, no appreciable change of the crystal structure occurs with ground WO_3, $(1-x)WO_{3-y}\cdot xReO_2$ mixtures and hydrogenated $CaWO_4$, whereas the presence of delocalized $5d^1$ electrons leads to phase transformations as is found in bronzes H_xWO_3.

Additionally, new bands located at about 950 and 970 cm^{-1} were found in ground WO_3 and $(1-x)WO_{3-y}\cdot xReO_2$ mixtures, respectively; the first was attributed to the tungsten–oxygen bonds at the free grains surface and the second one to crystal phase boundaries. The difference between the two cases is that in ground pure WO_3, the bonds are related to the W^{6+}–O^- or W^{6+}–OH groups whereas in $(1-x)WO_{3-y}\cdot xReO_2$ mixtures, they are related to the $W^{5.7+}$–O bonds. The unusually high frequency of the band is explained, in the first case, by the fact that vibrations are strongly localized at the surface of grains while, in the second case, the tungsten–oxygen bonds in $W^{5.7+}$–O–$2Re^{4+}$ group are expected to be stronger compared to the ones in W^{6+}–O–W^{6+} chains. One should point out that the position of the new bands is close to that observed in tungsten hydrates with double terminal W═O bonds.[28]

ACKNOWLEDGMENTS

The authors would like to thank Mrs. C. Armellini for the help in preparation of ground WO_3 samples and XRD measurements, Dr. E. Zanghellini for developing software for Raman data analysis and for useful discussions, Dr. A. Veispals for the preparation of $(1-x)WO_{3-y}\cdot xReO_2$ mixtures and Dr. A. DiCicco for supplying the x-ray absorption spectrum of ReO_2 reference compound. One of the authors (J.P.) wish to thank the LURE laboratory (Orsay) for the support of the XAS measurements. A.K. and J.P. are grateful to the Consiglio Nazionale delle Ricerche (Italy) and the Università di Trento for hospitality and financial support.

[1] C. G. Granqvist, *Handbook on Inorganic Electrochromic Materials* (Elsevier Science, Amsterdam, 1995).
[2] V. E. Henrich and P. A. Cox, *The Surface Science of Metal Oxides* (Cambridge University Press, Cambridge, 1994).
[3] J. B. Goodenough, Prog. Solid State Chem. **5**, 145 (1971).
[4] T. Iwai, J. Phys. Soc. Jpn. **15**, 1596 (1960).
[5] C. G. Granqvist, Appl. Phys. A: Solids Surf. **57**, 3 (1993).
[6] S. K. Deb, Appl. Opt. **3**, 192 (1969).
[7] C. G. Granqvist, Solid State Ionics **53/56**, 479 (1992).
[8] C. Bechinger, D. Ebner, S. Herminghaus, and P. Leiderer, Solid State Commun. **89**, 205 (1994).
[9] C. Bechinger, G. Oefinger, S. Herminghaus, and P. Leiderer, J. Appl. Phys. **74**, 4527 (1993).
[10] S. K. Deb, Philos. Mag. **27**, 801 (1973).

[11] I. Lefkowitz, M. B. Dowell, and M. A. Shields, J. Solid State Chem. **15**, 24 (1975).
[12] E. Salje, A. F. Carley, and M. W. Roberts, J. Solid State Chem. **29**, 237 (1979).
[13] E. Cazzanelli, G. Mariotto, C. Vinegoni, A. Kuzmin, and J. Purans, in *Electrochromic Materials and Their Applications III*, edited by K. C. Ho, C. B. Greenberg, and D. M. MacArthur, [Proc. Electrochem. Soc. **96-24**, 260 (1996)].
[14] P. G. Dickens and R. J. Hurditch, Nature (London) **251**, 1266 (1967).
[15] F. H. Jones, K. Rawlings, J. S. Foord, R. G. Egdell, J. B. Pethica, B. M. R. Wanklyn, S. C. Parker, and P. M. Oliver, Surf. Sci. **359**, 107 (1996); F. H. Jones, K. Rawlings, J. S. Foord, P. A. Cox, R. G. Egdell, J. B. Pethica, and B. M. R. Wanklyn, Phys. Rev. B **52**, R14 392 (1995).
[16] F. H. Jones, K. Rawlings, S. C. Parker, J. S. Foord, P. A. Cox, R. G. Egdell, and J. B. Pethica, Surf. Sci. **336**, 181 (1995).
[17] A. Kuzmin and J. Purans, J. Phys.: Condens. Matter **5**, 2333 (1993).
[18] A. Kuzmin, Physica B **208&209**, 175 (1995); A. Kuzmin, J. Phys. IV **7**, C2-213 (1997).
[19] A. Kuzmin, J. Purans, G. Dalba, P. Fornasini, and F. Rocca, J. Phys.: Condens. Matter **8**, 9083 (1996).
[20] H. P. Klug and L. E. Alexander, *X-ray Diffraction Procedures for Polycrystalline and Amorphous Materials* (Willey, New York, 1974).
[21] S. Laruelle and M. Figlarz, J. Solid State Chem. **111**, 172 (1994).
[22] P. M. Woodward, A. W. Sleight, and T. Vogt, J. Phys. Chem. Solids **56**, 1305 (1995).
[23] R. Diehl, G. Brandt, and E. Salje, Acta Crystallogr., Sect. B: Struct. Crystallogr. Cryst. Chem. **34**, 1105 (1978).
[24] P. G. Dickens, J. H. Moore, and D. J. Neild, J. Solid State Chem. **7**, 241 (1973); C. Genin, A. Driouiche, B. Gerand, and M. Figlarz, Solid State Ionics **53-56**, 315 (1992).
[25] E. Salje, Acta Crystallogr., Sect. B: Struct. Crystallogr. Cryst. Chem. **33**, 574 (1977).
[26] S. P. S. Porto and J. F. Scott, Phys. Rev. B **157**, 716 (1967).
[27] L. N. Limarenko, A. E. Nosenko, and M. V. Pashkovskii, *Influence of Structural Defects on the Physical Properties of Tungstates* (Visha Shkola, Lvov, 1978).
[28] M. F. Daniel, B. Desbat, J. C. Lessegues, B. Gerand, and M. Figlarz, J. Solid State Chem. **67**, 235 (1987).